Frenkel excitons in $NaNO_2$: excitation energy transfer and exciton coherence

1996 J. Phys.: Condens. Matter 8 115

(http://iopscience.iop.org/0953-8984/8/2/003)

J. Phys.: Condens. Matter **8** (1996) 115–141. Printed in the UK

REVIEW ARTICLE

Frenkel excitons in $NaNO_2$: excitation energy transfer and exciton coherence

Jürgen Köhler† and Dankward Schmid

Heinrich-Heine Universität Düsseldorf, Lehrstuhl für Festkörperspektroskopie (IPkM), Universitätsstrasse 1, 40225 Düsseldorf, Germany

Received 4 September 1995

Abstract. A review is presented about sensitized luminescence and luminescence lineshape studies on pure and doped sodium nitrite which have led to detailed knowledge about the lowest excited states of this system. Both the lowest triplet state and the first excited singlet state are Frenkel excitons, states that can migrate through the crystal. This migration is appropriately described by a one-dimensional energy transfer process for the triplet and, surprisingly, also for the singlet state. The exciton states themselves show an evolution in time that reveal the transition from coherent to incoherent behaviour with increasing temperature. In combination with theoretical investigations a consistent picture of the exciton states in sodium nitrite is achieved.

Contents

1. Introduction

The exciton model as developed by Frenkel [1] and Davydov [2] plays an important role in understanding processes concerning the transfer of excitation energy in biological systems.

† Present address: Leiden University, Huygens Laboratory, Centre for the Study of Excited States of Molecules, PO Box 9504, 2300 RA Leiden, The Netherlands.

0953-8984/96/020115+27$19.50

Because these systems are very complex, model systems are investigated for which it is hoped that the energy transfer processes are closely related to those in biology. The most intensively investigated model systems are organic molecular crystals [3–9]. In these systems the intramolecular interactions are much stronger than the intermolecular forces. This leads to a description of the crystals based on the molecular properties where the interaction between the molecules is taken into account as a small perturbation. The periodic crystal structure causes delocalized excited states—excitons—which give rise to excitation energy transfer from lattice site to lattice site. The exciton states are linear combinations of localized excited states. To study the energy transfer by excitons pure crystals are doped with a small amount of impurities which have excited states lower in energy than the host crystal. Excitons migrating through the crystal can be trapped at the impurities and studying the trap luminescence yields insights into the exciton dynamics. However, in this case it is almost impossible to distinguish between the motional properties of the excitons and the capture process at the trap site.

During the last few years a detailed picture of the lowest excited states of sodium nitrite ($NaNO_2$) has been obtained. It turns out that $NaNO_2$ is a suitable system to investigate the excitation energy transfer via excitons and that insights into the description of exciton motion are obtainable. When Frenkel studied the excitations of crystals theoretically he called the states which now are commonly called Frenkel excitons 'excitation waves', which refers to their wavelike character. However this description only holds for ideal crystals at absolute zero temperature. Interactions with lattice imperfections or vibrations will cause the formation of exciton wave-packets moving through the crystal in a diffusive way. By studying the spectral lineshapes of the luminescence transitions in $NaNO_2$ it was possible to observe the change from wavelike (coherent) to diffusive (incoherent) exciton motion.

After a brief description of the exciton model the first part of this contribution will cover the energy transfer experiments while the coherence properties of the excitons are the subject of the second part.

2. Frenkel excitons

The exciton model was developed by Frenkel [1] and Davydov [2]. It describes the transfer of excitation energy in crystals from lattice site to lattice site without transport of charge or mass. A detailed description of the model can be found in [2] and [10]. If a photon with energy ν_i and momentum $\hbar \boldsymbol{k}_{photon}$ is absorbed by the crystal an exciton of the same energy and quasimomentum is created. The exciton describes a collective excitation of the whole crystal and its wave-function is given by a Bloch state:

$$|k\rangle = \frac{1}{\sqrt{N}} \sum_n \mathrm{e}^{\mathrm{i}kr_n} |r_n\rangle \tag{1}$$

where $|r_n\rangle$ denotes the state of a single excited molecule at lattice site r_n and all other $(N-1)$ molecules in the ground state; $\boldsymbol{k}$ is the exciton wave-vector and the sum runs over all lattice sites. The energy of the exciton forms a quasicontinuous band structure which is given by

$$\varepsilon(k) = \sum_{n \neq m} \beta_{nm} \mathrm{e}^{\mathrm{i}k(r_n - r_m)} \tag{2}$$

where β_{nm} is the interaction matrix element of molecules at lattice site n and m. In a perfect crystal at zero temperature the exciton will not change its initial momentum until it decays to the ground state. Everything that disturbs this ideal situation leads to a scattering among

the $\boldsymbol{k}$ states of the exciton band and finally thermalizes the exciton band. In real crystal systems the states associated with the exciton are represented by wave-packets of Bloch states:

$$|\Psi_{exciton}\rangle = \int g(k - k_0)|k\rangle \, \mathrm{d}k \tag{3}$$

where $g(\boldsymbol{k}-\boldsymbol{k}_0)$ is a weighting function. If the temperature is sufficiently low, which means that the interaction of excitons and phonons is still weak, the wave-function of the exciton, $|\Psi_{exciton}\rangle$, is centred around a mean value $\boldsymbol{k}_0$ with a width Δk which is small compared to the dimensions of the Brillouin zone. This means that the average time between two scattering events is long compared to h/β_{nm}. In this case the exciton is called coherent, and the energy transfer through the crystal is wavelike. This implies that the distribution of $\boldsymbol{k}$ states of the wave-packet does not change significantly during the propagation of the excitation through the crystal. Raising the temperature and equivalently increasing the exciton–phonon interaction will lead to a growing scattering rate among the exciton $\boldsymbol{k}$ states resulting in a change of the average value $\boldsymbol{k}_0$ and the width Δk of the wave-packet. According to the uncertainty relation $\Delta x \Delta k \geq 2\pi$ the width of the wave-packet Δk is related to the region of localization Δx of the excitation which decreases with increasing width of the wave-packet. When Δx approaches the order of the lattice constant the excitation becomes localized and its motion through the crystal can be visualized as a random walk from lattice site to lattice site. This is referred to in the literature as an incoherent exciton. Whether the energy transfer in a specific system is coherent or incoherent depends on the competition between the excitation transfer and the scattering processes.

It is interesting to obtain experimental information about the strength of the interaction matrix element β_{nm}, which determines the efficiency of the energy transfer process and whether the transfer of excitation energy is anisotropic. Another interesting point concerns the description of the excitations themselves: do they behave as (partly) coherent excitons or as randomly hopping wave-packets?

3. The system $NaNO_2$

3.1. The crystal structure

$NaNO_2$ is an intermediate between van der Waals crystals and pure ionic systems. At room temperature it has a body centred orthorhombic lattice structure with two formula units of four atoms per conventional unit cell [11]. The unit cell is sketched in figure 1(*a*), where each sphere represents an $NaNO_2$ molecule as shown in figure 1(*b*). The lattice parameters are $a = 356.78$ pm, $b = 575.84$ pm and $c = 539.19$ pm [13]. The NO_2^- molecular ions are stacked along the short a axis while adjacent stacks are separated from each other by the Na^+ ions. The NO_2^- molecules have a permanent dipole moment of 0.21 debye [14] (0.70×10^{-30} C m) and are aligned along the b axis, causing the ferroelectricity of the crystal. At $T_c = 436.6$ K a phase transition into an antiferroelectric phase occurs. This exists only in a very small temperature interval, and for temperatures above $T_N = 437.5$ K, $NaNO_2$ becomes paraelectric [13]. With its four atoms per primitive unit cell, $NaNO_2$ has 12 phonon branches. The three modes highest in energy are assigned to the intramolecular vibrations of the NO_2^- ion [15, 16]. They will be discussed in more detail in later sections of this article. The lower-energy intermolecular modes have been investigated by various experimental techniques such as Raman and infrared spectroscopy [16–26], reflection spectroscopy [27–30] and inelastic neutron scattering [31, 32]. Additional information about the phonons, especially the density of states of the acoustic modes, was obtained by studying the specific

heat [33]. The conclusion was that for temperatures between 300 mK and 20 K $NaNO_2$ behaves like a Debye solid ($c_p \sim T^3$) with a Debye temperature of $\theta_D = (345 \pm 10)$ K. A definite model for the phase transition has not been established yet. However, agreement exists that it is not caused by a soft mode.

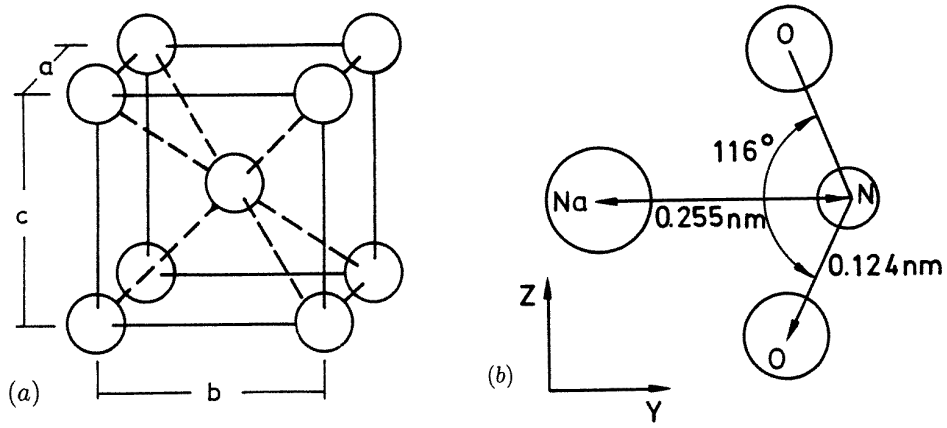

Figure 1. (*a*) The conventional unit cell of an $NaNO_2$ crystal. Each sphere represents an $NaNO_2$ molecule as shown in (*b*). (*b*) The dimensions of the $NaNO_2$ molecule [12]. The molecular x, y and z axes are parallel to the crystal a, b and c axes, respectively.

3.2. The photoexcited states

The lowest unoccupied electronic states of $NaNO_2$ are the $^3B_1$ triplet state and the $^1B_1$ single state of the NO_2^- molecule [34]. The absorption of the crystal in the near UV is caused by the $^1B_1 \leftarrow {}^1A_1$ transition [15]. Exciting $NaNO_2$ into higher vibrational states of the $^1B_1$ state is followed by a fast vibronic relaxation on a time scale of picoseconds [35, 36]. The molecule can decay back to the ground state or cross over to the $^3B_1$ triplet level by a radiationless intersystem crossing (ISC) process. The ISC becomes possible due to perturbations such as spin–orbit coupling, which mixes some singlet character into the triplet state and vice versa [37, 38]. The decay of the singlet state $^1B_1 \rightarrow {}^1A_1$ yields a fluorescence in the blue spectral region, while the radiative decay of the $^3B_1$ triplet state causes a weak phosphorescence in the green spectral regime. The ratio of the fluorescence to the phosphorescence intensity is about 100:1 but depends on the excitation energy owing to the competition between the vibronic relaxation and the ISC [39]. Both states have been studied in great detail and will be described briefly in the following.

3.2.1. The triplet state. The $^3B_1$ triplet state of $NaNO_2$ can decay radiatively to the $^1A_1$ ground state resulting in a weak phosphorescence, which was observed for the first time by Maria *et al* [40]. A detailed analysis of the spectrum was given by Hochstrasser and Marchetti [41]. Like the absorption spectrum, the phosphorescence shows a vibrational structure which results from the coupling of the electronic transition of the NO_2^- to the vibrational modes of the $^1A_1$ electronic ground state. The energy of the pure electronic transition has been determined as $\nu_{00}^{triplet} = 18\,959$ cm^{-1} [41]. The generating frequencies of the progressions are the same as observed in fluorescence and will be discussed in the next section. From the $^3B_1 \leftarrow {}^1A_1$ absorption spectrum the NO_2^- vibrational frequencies in the

triplet state have been determined as $\nu_1 = 1124$ cm^{-1} (symmetric stretch), $\nu_2 = 644$ cm^{-1} (symmetric bending) and $\nu_3 = 1170$ cm^{-1} (asymmetric stretch) [42] in close agreement to the values reported in [43]. The origin of the spectrum coincides with the 18 959 cm^{-1} observed in phosphorescence. Due to its total electronic spin of $S = 1$, the triplet state can be investigated by magnetic resonance methods. It is a well known feature that molecular systems show in zero external magnetic field a so-called zero-field splitting. The dipole–dipole interaction of the two unpaired electrons lifts the degeneracy of the three triplet sublevels, t_x, t_y and t_z. This interaction is diagonal for axes fixed to the molecular as shown in figure 1(*b*). The theory and methods to observe and interpret magnetic resonance transitions is well known [44, 45]. Here only a summary of the results will be presented. For $NaNO_2$, Dietrich *et al* [42, 46–48] determined the zero-field parameters to be $D = (0.4480 \pm 0.0007)$ cm^{-1} and $E = -(0.047\,79 \pm 0.000\,02)$ cm^{-1}. As mentioned already the triplet state is populated by the radiation-less ISC process which is possible due to small perturbations. These perturbations, like spin–orbit coupling, are very selective with respect to the triplet sublevels leading to significant differences in the populations of the three substates. For $NaNO_2$ the t_x level is populated preferentially. For the decay of the sublevels to the ground state, again two electronic states of different multiplicity are coupled, resulting in different lifetimes for the three sublevels. Dietrich *et al* obtained for the respective lifetimes $\tau_x = 0.41$ ms, $\tau_y = 0.46$ ms and $\tau_z = 0.1$ ms and showed that only the t_y level has a radiative decay path. Thus the observed phosphorescence results from the decay of the t_y level. It is populated via the t_x level by spin–lattice relaxation which in this particular case is a rather slow process (≈ 1 ms). Therefore no thermal equilibrium between the sublevels is established during the triplet lifetime. The t_z level, which has the shortest lifetime, decays to the ground state nonradiatively.

3.2.2. The singlet state. The $^1B_1 \leftarrow {}^1A_1$ absorption spectrum shows a vibrational structure and the energy of the pure electronic transition is $\nu_{00}^{singlet} = 25\,975$ cm^{-1}. Two progressions can be observed with generating frequencies of 620 cm^{-1} and 1020 cm^{-1} [26]. They were assigned to the intramolecular bending mode and the intramolecular symmetric stretching mode of the nitrite molecule in the first singlet state. The fluorescence caused by the decay of the $^1B_1$ state to the ground state was observed as early as 1934 by Rodloff [49] and attracted much attention later on. The fluorescence spectrum, shown in figure 2, shows progressions due to the coupling of the $^1B_1 \rightarrow {}^1A_1$ electronic transition of the nitrite to the intramolecular vibrational modes of the electronic ground state. The positions of the fluorescence lines observed are given approximately by

$$\nu_{nm} = \nu_{00} - n\nu_1 - m\nu_2 \tag{4}$$

where $\nu_{00} = 25\,975$ cm^{-1} [50] denotes the energy of the pure electronic transition, $\nu_1 = 1325$ cm^{-1} [42] is the energy of the symmetric stretching vibration of the NO_2^- and $\nu_2 = 830$ cm^{-1} [51] is the energy of the corresponding symmetric bending vibration. The lifetime of this state has been determined to be 8 ns [52]. The broad appearance of this spectrum is well understood on the basis of an oriented gas model.

4. Excitation energy transfer: doped $NaNO_2$ crystals

4.1. Theoretical concept

If a crystal is doped with a small amount of a suitable dopant this may lead to perturbed centres in the crystal having excited state energies below the exciton band. As a consequence

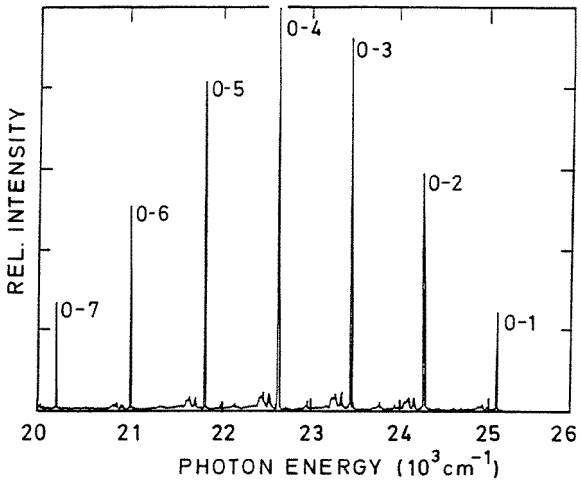

Figure 2. The fluorescence spectrum of $NaNO_2$ at 4.2 K. The crystal was excited in the UV with a broad-band mercury arc light source.

the exciton can be trapped at such a lattice site. Due to the population of the traps by energy transfer, their respective transitions show up in the spectrum as much more intense than expected from the concentration ratio. This phenomenon is known as sensitized luminescence [3]. Investigating this allows information on the transfer of excitation energy to be obtained. For the interpretation of the energy transfer data, a generalized master equation (GME) approach has been shown to be a useful concept. Kenkre and coworkers, who developed this formalism [53–61], obtained expressions for the rates involved in the energy transfer process independent of the degree of exciton coherence. For the so-called energy transfer rate, k_{HG}, from the host to the guest system the expression

$$1/k_{HG} = 1/M + 1/C - \rho\tau_H^0 \tag{5}$$

was found where M denotes the motion rate of the exciton, C the capture rate at the trap, ρ the trap concentration and τ_H^0 the lifetime of the excited state for the pure host system. From expression (5) it follows that k_{HG} does not exclusively carry information about the exciton motion. The transfer rate is determined mainly by the exciton motion and the capture process at the trap site whereas $\rho\tau_H^0$ usually is small. The slower process forms the bottleneck for the total transfer of excitation energy to the trap. The energy transfer can be described by a phenomenological rate equation system [3, 5, 53] which leads to an expression for the energy transfer rate which is directly related to experimental observables. For steady state conditions one obtains for k_{HG}

$$k_{HG} = (1/\rho\tau_H^0)\Phi_G/\Phi_H \tag{6}$$

where Φ_G/Φ_H is the guest to host quantum yield ratio. For the initial condition of pulsed excitation an expression

$$k_{HG} = (1/\rho)(1/\tau_H - 1/\tau_H^0) \tag{7}$$

is found where τ_H^0 is the excited state lifetime of the pure host system whereas τ_H is the excited state lifetime of the host in the presence of the dopant. In this way two experimental approaches are available to determine k_{HG}.

Another interesting parameter described by the GME theory is the exciton–exciton annihilation rate γ, which takes account of the fact that at high excitation density the excitons can interact with each other. In a simplified picture one can imagine that two excitons will meet each other and create a higher excited state. Thus two excitons disappear. They are annihilated, which is described by

$$1/\gamma = 1/M + 1/D \tag{8}$$

where M again is the motion rate and D is the destruction rate.

As can be seen from equations (5) and (8) the energy transfer rate k_{HG} as well as the annihilation rate γ carry information about the exciton motion represented by the rate M. M is the parameter which describes the energy transfer process within the manifold of host molecules. In the GME approach the rate M depends on whether the exciton can move in one, two or three dimensions [55].

$$M = \sqrt{(1 + 4F\tau_H^0)}/\tau_H^0 \approx \sqrt{(4F/\tau_H^0)} \qquad \text{one dimension} \tag{9}$$

$$M = (4\pi F)/\ln(32F\tau_H^0) \qquad \text{two dimensions} \tag{10}$$

$$M = 3.96F\left(1 + 0.32/\sqrt{(F\tau_H^0)}\right) \approx 4F \qquad \text{three dimensions} \tag{11}$$

The approximations are valid for $F\tau_H^0 \gg 1$ where F denotes the so-called hopping rate. The name results from the visualization of an exciton randomly hopping from lattice site to lattice site. Because (9)–(11) are independent of the degree of exciton coherence, F^{-1} should be interpreted as the time that a wave-packet, formed by the exciton Bloch states, needs to move by one lattice site.

4.2. Triplet excitons

For $NaNO_2$ crystals doped with KNO_2 the phosphorescence spectrum shows additional narrow lines due to perturbed NO_2^- molecules close to the potassium ion. These perturbed NO_2^- molecules act as traps for the excitons and form the 'guest' molecules in the doped crystal system. The situation is reminiscent of the so-called X traps in organic molecular crystals [3, 62, 63], which are molecules of the host crystal whose excitation energy is lowered due to the perturbation by the presence of a guest molecule. Talking about traps or guests in the context of this article therefore means X traps. Dietrich *et al* observed the magnetic resonance spectra of these molecules in comparison with the unperturbed ones. For a localized state one would expect a hyperfine interaction of the electronic triplet spin with the ^{14}N nuclear spin ($I = 1$). Indeed this has been observed for the trap states but not for those of the unperturbed molecules [46, 48]. The explanation for this phenomenon is given by a motional narrowing process due to the nonlocalized character of the host triplet state. The hyperfine interaction is averaged out due to the mobility of the excited state. Further information was obtained from optical experiments by Schmidt *et al* [64, 65], who studied the so-called delayed fluorescence on pure crystals. When the excitation density is sufficiently high (annihilation regime), two triplet excitons can create a higher excited state. This state will most probably relax to the $^1B_1$ singlet state and decay radiatively to the ground state. In this way fluorescent light in the blue spectral region can be obtained. Because the triplet–triplet annihilation lasts for a long time compared to the singlet lifetime, it is delayed with respect to the ordinary, directly excited fluorescence. Schmidt *et al* showed a quadratic dependence of the delayed fluorescence intensity on the excitation power which proved the mutual annihilation of two excited triplet states. They

also studied the temperature dependence of the intensity of the delayed fluorescence and observed an increase up to about 30 K followed by a sudden drop at higher temperatures (see figure 3(*a*)). Figure 3(*b*) shows the temperature dependence of the energy transfer rate k_{HG} as obtained from equation (6) from sensitized phosphorescence experiments on $NaNO_2$ crystals doped with KNO_2 [51]. The two temperature dependences show remarkable similarities. From equations (5) and (8) Lisse *et al* [51] concluded therefore that both processes, the annihilation as well as the host to guest energy transfer, are dominated by the exciton motion. Assuming $k_{HG} \approx M$ and using $F = 10^9\ s^{-1}$ as determined by Dietrich *et al*, one can compare the value for k_{HG} obtained experimentally with the predictions of the GME theory. Using equations (9)–(11), one obtains $M = 6 \times 10^6\ s^{-1}$ (one dimension), $M = 8 \times 10^8\ s^{-1}$ (two dimensions) and $M = 4 \times 10^9\ s^{-1}$ (three dimensions). Lisse *et al* [51] obtained experimentally $k_{HG} \approx M \approx 5 \times 10^6\ s^{-1}$ for a crystal temperature of 4.2 K. Based on the agreement of the experimental value of M and that calculated for a one-dimensional motion it was concluded that for triplet excitons the motion takes place in a one-dimensional fashion [51, 52]. This conclusion seems to be reasonable since in $NaNO_2$ the NO_2^- ions are stacked along the short crystallographic a axis, and since for triplet excitons only the short-range exchange interaction is relevant. However, the number of traps produced in the crystal for a given K^+ concentration as well as the ratio of the dopant concentration in the melt to that in the solid is not known. Presumably the ratio of both is of the order of one, but it should be kept in mind that the conclusion mentioned above is based on rough estimates.

4.3. Singlet excitons

The much stronger fluorescence of $NaNO_2$ caused by the radiative decay of the $^1B_1$ singlet exciton has been studied intensively by several authors. In this section only experiments concerning the excitation energy transfer in the singlet state will be described. For $NaNO_2$ doped with KNO_2 a sensitized fluorescence study has been performed in great detail [51, 52, 64, 65, 67]. The perturbed NO_2^- ions close to the K^+ ion form a trap system of at least three pairs of deep and shallow traps interacting with each other. To obtain the singlet energy transfer rate Pufahl *et al* [52] followed two independent experimental strategies. Using equations (6) and (7), k_{HG} was determined by pulsed excitation and by steady state experiments. For the calculation of k_{HG} from the experimental data Pufahl *et al* determined the actual dopant concentration in the crystal by comparison of fluorescence quantum yields with standard samples. It must be emphasized that in this way the concentration of the K^+ ions was determined rather than the actual concentration of the perturbed NO_2^- molecules. Schmidt *et al* [67] showed that about five traps per K^+ ion were formed, which multiplies the number of K^+ ions by this factor to obtain the 'real' trap concentration in the crystal. Figure 4 shows the energy transfer rate k_{HG} obtained experimentally. The solid line gives the result from pulsed excitation experiments analysed using equation (7) while the broken line gives the result from the steady state experiments according to equation (6). In both cases the K^+ concentration has been used for ρ. The agreement between the two independent experimental results carried out on different set-ups and using different samples is satisfactory. To obtain a realistic value for the transfer rate normalized to the trap concentration the experimental value has to be divided by a factor of five. For a crystal temperature of 4.2 K k_{HG} has been reported to be $1.0 \times 10^{10}\ s^{-1}$ [52].

Pufahl *et al* also determined the annihilation rate γ for the singlet state. Therefore the decay rates of the singlet state for high excitation density were measured and the respective phenomenological second-order rate equation system was solved numerically

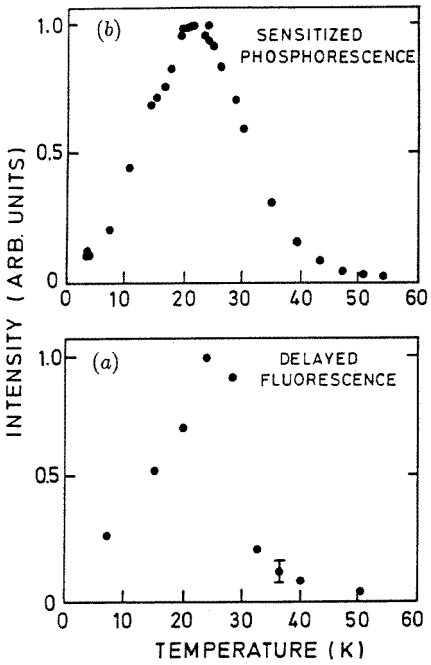

Figure 3. (*a*) The temperature dependence of the relative intensity of the delayed fluorescence [65]. (*b*) The temperature dependence of the triplet energy transfer rate according to (6) [51]. For better comparison both graphs are normalized.

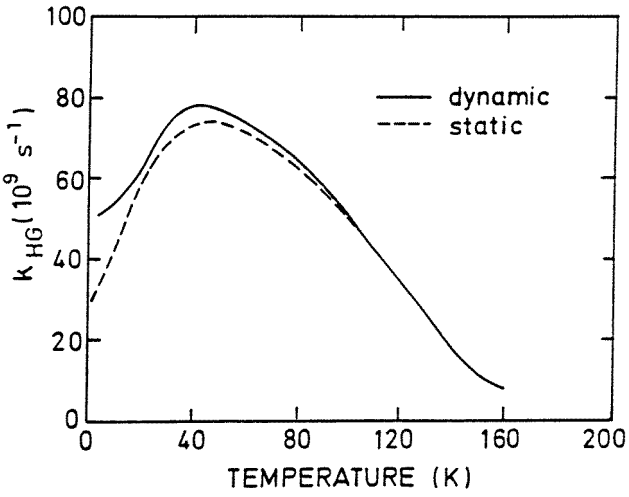

Figure 4. The temperature dependence of the singlet energy transfer rate according to (7)—full line—and (6)—broken line. For the concentration, ρ, the amount of K^+ has been used [52].

[52]. The annihilation rate obtained in this way shows qualitatively the same temperature dependence as the host–guest energy transfer rate. It was concluded that also in the singlet state the energy transfer is motion limited and as before the approximation $k_{HG} \approx M$ was

used. Using (9)–(11) this yields for the hopping rates $F = 2 \times 10^{11}$ s^{-1} (one dimension), $F = 3.9 \times 10^{6}$ s^{-1} (two dimensions) and $F = 2.5 \times 10^{9}$ s^{-1} (three dimensions), respectively. As will be shown in section 5 the singlet excitons in $NaNO_2$ behave coherently at low temperatures [68–70]. For this case the hopping rate is directly related to the width of the exciton band. Expressing the bandwidth in units of (E/hc) one obtains for the one-dimensional case $\Delta\nu_{ex} \approx 6.6$ cm^{-1} in good agreement with the value of 5 cm^{-1} obtained from a lineshape analysis. Analogous model calculations for two or three dimensions yielded results orders of magnitude too small to be consistent with the lineshapes observed.

At first glance one might be surprised about the one-dimensional character of singlet excitons because in the singlet manifold the strong, long-range Coulomb interaction also contributes to the transfer matrix element, but it should be realized that the $^1B_1 \leftarrow {}^1A_1$ transition in $NaNO_2$ is weak for an allowed transition. The transition dipole moment is relatively small (oscillator strength, $f \approx 2.5 \times 10^{-5}$ [71]), causing the singlet exciton bandwidth of only 5 cm^{-1}, which is a value more typical for triplet excitons. Given the orbital structure of the $^1B_1$ state, which is proposed to be composed of p-type atomic orbitals on the nitrogen and oxygen atoms with a nodal plane perpendicular to the a axis [72], and keeping in mind the anisotropic crystal structure this is a reasonable result.

5. The singlet exciton

5.1. The exciton bandstructure

Exciting $NaNO_2$ in the UV spectral region with a broad-band light source yields the fluorescence spectrum as presented in figure 2. The narrow lines of this spectrum result from the coupling of the $^1B_1 \rightarrow {}^1A_1$ transition to the intramolecular vibrations of the electronic ground state. These intramolecular vibrations are delocalized crystal phonons and are usually referred to as vibrons or vibrational excitons. The observed transitions in the spectrum will be termed '$(0\text{–}n\nu_x)$ transitions', where ν_x gives the respective vibrational mode and n the number of vibrational quanta involved. Recording these transitions with enhanced spectral resolution resolves asymmetric lineshapes as first observed by Schmidt [64]. All members of the progression show lineshapes which are very similar in their gross appearance leaving some details slightly different [51]. The shape of these lines is illustrated in figure 5(a) for the example of the $(0\text{–}1\nu_2)$ transition [73].

To explain the lineshape Lisse proposed that the exciton and the vibron dispersion had to be taken into account [51]. The excitation in the UV creates highly excited electronic states. After a fast relaxation the system will be prepared in the $^1B_1$ exciton state. Due to the numerous scattering events which cause the relaxation all exciton $\boldsymbol{k}$ states will be populated. The subsequent radiative decay of the exciton has to obey the $\boldsymbol{k}$ conservation rule.

$$k_{exciton} + k_{photon} = k_{vibron}. \tag{12}$$

Here and in the following the $\boldsymbol{k}$ vector of the photons can be neglected; therefore, the lineshape was ascribed to the dispersion of the exciton and that of the vibron. It was shown that, consistent with this interpretation, spectral lines caused by localized states, which do not show dispersion, are symmetrical in shape [73]. This was first observed for transitions originating from NO_2^- ions perturbed by close K^+ impurities, which showed Lorentzian shaped lines [51, 74], and it will be illustrated in the following on the example of isotopically substituted molecules. The natural abundance of the rare isotopes ^{15}N, ^{17}O and ^{18}O is 0.37%, 0.037% and 0.204%, respectively. They cause three additional weak

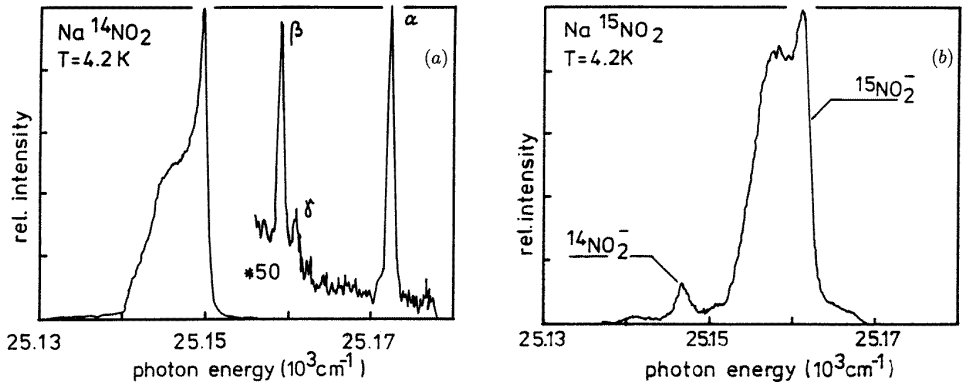

Figure 5. The spectral region of the $(0–1\nu_2)$ fluorescence transition for two $NaNO_2$ crystals of different isotopical constitution. Both spectra were recorded at 4.2 K [73]. (*a*) Natural abundance. The lines marked α, β and γ are caused by NO_2^- molecules containing the isotopes of ^{18}O, ^{15}N and ^{17}O, respectively. To record these lines the sensitivity of the detection system was increased by a factor of 50 with respect to the main fluorescence transition. (*b*) $NaNO_2$ enriched to 99% with ^{15}N. The spectrum shows the same spectral region as part (*a*).

progressions in the spectrum which can be distinguished from the 'master line' because the pure electronic transition frequency and the generating mode frequency are slightly different [75, 76]. In figure 5(a) the lines denoted α, β and γ, which were recorded with increased sensitivity, originate from $^{14}N\,^{18}O\,^{16}O^-$ (α), $^{15}N\,^{16}O_2^-$ (β) and $^{14}N\,^{17}O\,^{16}O^-$ (γ) ions in natural abundance. Members of the α and β progressions showed Lorentzian shaped lines with a width of 0.5 cm^{-1} (FWHM) [74]. The translational invariance, which caused the formation of exciton Bloch states, is not given for these molecules. They do not participate in the bandstructures and consequently do not 'feel' dispersion. Their lineshapes prove that the shape of the 'master line' is not an intrinsic property of the NO_2^- ion but a collective effect. Stimulated by this observation a crystal with nearly reversed abundancies of ^{14}N and ^{15}N was studied. In figure 5(*b*) the same spectral region as in part (*a*) of the figure is shown for a crystal enriched with ^{15}N to a degree of 99% [70, 73]. Obviously for this case the $^{15}NO_2^-$ transitions show the characteristic asymmetry while the $^{14}NO_2^-$ ions show up with a symmetric lineshape in the fluorescence spectra.

By comparing the linewidth of transitions that involve either the triplet or the singlet exciton and the ν_1 or ν_2 vibron, boundaries for the width of the singlet exciton and ν_2 vibron bandstructures were obtained [68]. For the $(0–1\nu_2)$ triplet transition ($^3B_1 \rightarrow {}^1A_1$), which involves the triplet exciton in the initial state and the ν_2 vibron in the final state, an asymmetric lineshape was observed with a width of about 3 cm^{-1}. From the oscillator strength of the triplet state (10^{-10}–10^{-12}) [46] the bandwidth of the triplet exciton was estimated to be less than 0.1 cm^{-1}, which is due to the small exchange interaction in the triplet state. Therefore the observed linewidth of 3 cm^{-1} was ascribed completely to the ν_2 vibron band. The width of the $(0–1\nu_2)$ singlet transition (figure 5(*a*)), however, was assumed to be influenced by both bandstructures involved because in the singlet state the stronger Coulomb interaction is relevant, too. This leads to an estimate for the singlet exciton bandwidth of 5 cm^{-1}.

More quantitative information about the vibron band was obtained by calculating the dispersion relation of the vibrational modes [77]. Lattice dynamics studies of $NaNO_2$ have been performed previously [31, 78–80]. Lynden-Bell *et al* [80] used a site–site potential and

studied $NaNO_2$ by classical molecular dynamics. Castellucci and Schettino [79] showed that the rigid-ion model was inadequate to reproduce the experimental frequencies and LO–TO splittings. They included the atomic polarizability by means of the shell model. Unfortunately none of the previous publications calculated the density of states of the vibrons to allow to calculate lineshapes for optical transitions. Janssen *et al* [77] modified the assumed charge distribution in such a way as to reproduce the experimentally observed LO–TO splittings of the vibron modes and took the atomic polarizabilities into account by means of the shell model as suggested by Castellucci and Schettino. For the calculations the experimental polarizabilities obtained from measurements of the refractive index were used [81]. To compare the calculated dispersion relation of the ν_2 vibron mode with experimental data the lineshape of the $(0–1\nu_2)$ fluorescence transition was calculated in the following way. They assumed a one-dimensional exciton bandstructure along the crystal *a* axis, which yields in nearest-neighbour approximation the well known cosine-type dispersion for the exciton energy. For the exciton bandwidth the value of 5 cm^{-1} was used. Because the exciton state is composed of $^1B_1$ molecular excited states which have a nodal plane perpendicular to the *a* axis, it was assumed that the exciton state at $k = 0$ is highest in energy. Calculating the density of states for the ν_2 vibron and the exciton band finally yielded the lineshape for the transition between these two bandstructures, which is compared in figure 6 with the experimental lineshape [77, 82]. The displayed experimental spectrum corresponds to a crystal temperature of 15 K because it is known that below this temperature the excitons are not distributed uniformly over the Brillouin zone [70] (see the next section). It must be emphasized that there was no free parameter for adjusting the calculation of the lineshape, which shows a good agreement with the observed spectrum.

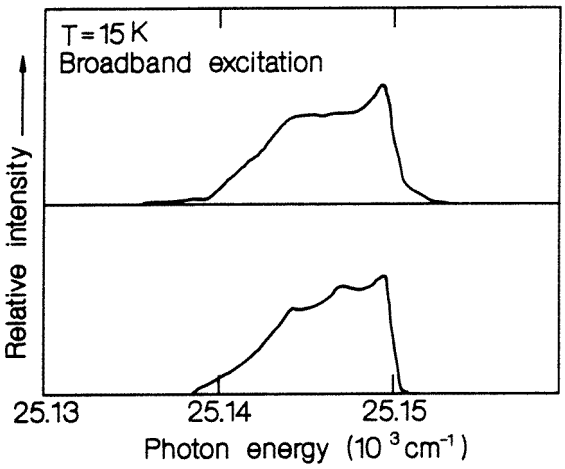

Figure 6. A comparison of the calculated lineshape of the $(0–1\nu_2)$ fluorescence transition (lower part) with the experimental one for a crystal temperature of 15 K (upper part) [82].

This result confirms that the observed fluorescence lineshapes are caused by the dispersion of the exciton and the vibron and that the exciton bandstructure is reasonably well approximated as one dimensional, consistent with the conclusions concerning the energy transfer.

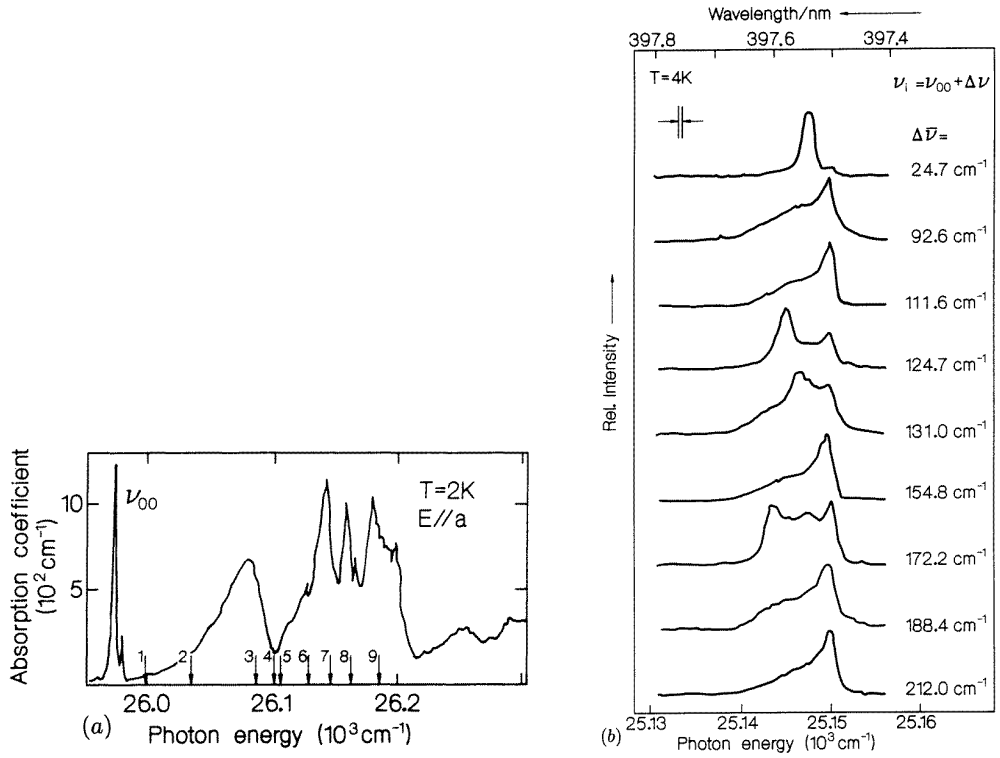

Figure 7. (*a*) The absorption spectrum of $NaNO_2$ close to the exciton resonance ν_{00}. The position of the excitation energies of part (*b*) of the figure are indicated by the arrows [50]. (*b*) The lineshape of the (0–1ν_2) fluorescence transition at 4.2 K for different excitation energies as indicated in (*a*). The incident laser frequency, ν_i, is given by the excess energy $\Delta\nu$ above the exciton resonance ν_{00} at 25 975 cm^{-1} [68].

5.2. The degree of exciton coherence

5.2.1. Steady state excitation. The degree of exciton coherence has been studied by Köhler *et al* [68–70] using fluorescence excitation spectroscopy and fluorescence spectroscopy with selective narrow-band excitation. Exciting the crystal near the exciton resonance energy with a laser creates excitons in distinct $\boldsymbol{k}$ states. It was investigated whether the excitons will conserve the initial $\boldsymbol{k}$ vector during their lifetime or will be scattered all over the exciton band. A significant dependence of the fluorescence lineshape of the (0–2ν_2) transition at $T = 2$ K on the exciting laser frequency was first observed by Sakai *et al* [83]. Köhler *et al* showed that the various lineshapes themselves depend on temperature. In figure 7(*a*) the absorption spectrum of $NaNO_2$ close to the exciton resonance is shown. The pure electronic transition, at ν_{00}, is accompanied by a broad structured phonon sideband which corresponds to an absorption process where an exciton and a crystal phonon are created simultaneously [50, 84]. In figure 7(*b*) the lineshape of the (0–1ν_2) transition for different excitation energies within the phonon sideband is shown. The incident photon energy of the laser, ν_i, is given in terms of the excess energy $\Delta\nu$, which is the amount of energy by which the laser exceeds the exciton resonance. The simultaneous creation of a crystal

phonon and an exciton has to obey momentum and energy conservation:

$$0 \approx k_{ex} + k_{ph} \tag{13}$$

$$\nu_i = \nu_{ex}(k_{ex}) + \nu_{ph}(k_{ph}). \tag{14}$$

The momentum of the photon has been neglected. The indices ex, ph and later on vib refer to exciton, phonon and vibron, respectively; ν_i is the incident photon energy. In this way an exciton with a certain $\boldsymbol{k}$ vector inside the Brillouin zone will be excited. However, because the phonon dispersion relation $\nu_{ph}(\boldsymbol{k}_{ph})$ is not necessarily a unique function of $\boldsymbol{k}_{ph}$, in fact many different phonon branches are overlapping, the excitons will be created in more than exactly one $\boldsymbol{k}$ state. Nevertheless the important point is that excitons were created in a finite number of distinct $\boldsymbol{k}$ states. The probability of this process depends on the density of states of the phonons and excitons at the respective $\boldsymbol{k}$ vectors determined by the energy conservation (14):

$$p_e \sim g_{ph}(k_{ph})g_{ex}(k_{ex}). \tag{15}$$

p_e denotes the probability of the excitation process and g refers to the respective density of states at a particular $\boldsymbol{k}$ state. In principle the excitons created in this way at $\boldsymbol{k}_{ex}$ can change their momentum to $\boldsymbol{k}'_{ex}$ by scattering events. Eventually this should lead to a thermal distribution for the population of the $\boldsymbol{k}$ states. Let the exciton scattering be described by the (unknown) function S. This function S describes that an exciton which is created in a state $\boldsymbol{k}_{ex}$ will be scattered into a state $\boldsymbol{k}'_{ex}$. S will depend on many parameters, for instance the crystal temperature, but a boundary condition which is known definitely is that in the limit of a very fast scattering time, $\tau_{\boldsymbol{k}\boldsymbol{k}'}$, S has to lead to an exciton population in thermal equilibrium. The interesting question is whether the exciton lifetime is sufficiently long (or the scattering sufficiently fast) that a thermal equilibrium can be established. The function S will be written here as $S(\boldsymbol{k}_{ex}, \boldsymbol{k}'_{ex})$ to indicate that it gives the redistribution of exciton $\boldsymbol{k}$ states. The lifetime of the singlet exciton is 8 ns. To keep things general it is assumed that the exciton will decay to the ground state from the state $\boldsymbol{k}'_{ex}$. Whether $\boldsymbol{k}'_{ex}$ is identical to the state $\boldsymbol{k}_{ex}$ populated initially depends on $S(\boldsymbol{k}_{ex}, \boldsymbol{k}'_{ex})$. Obeying energy and momentum conservation for the decay process into an (electronic ground state) vibron yields

$$k'_{ex} = k_{vib} \tag{16}$$

$$\nu_d = \nu_{ex}(k'_{ex}) - \nu_{vib}(k_{vib}) \tag{17}$$

where ν_d represents the energy of the photon emitted during this process (d for detection). The probability for this process is proportional to the vibron density of states and the respective exciton density of states:

$$p_d \sim g_{vib}(k_{vib})g_{ex}(k'_{ex}). \tag{18}$$

The experimental interest lies in the conditional probability of creating an exciton at $\boldsymbol{k}_{ex}$ and of detecting a decay at $\boldsymbol{k}'_{ex}$. The signal as a function of ν_i, ν_d, $\boldsymbol{k}_{ex}$, $\boldsymbol{k}'_{ex}$, $\boldsymbol{k}_{ph}$ and $\boldsymbol{k}_{vib}$ is given by

$$\begin{aligned} m_0 \sim\ & g_{ph}(k_{ph})g_{ex}(k_{ex})S(k_{ex'}k'_{ex})g_{vib}(k_{vib})g_{ex}(k'_{ex})\delta(\nu_i - [\nu_{ex}(k_{ex}) + \nu_{ph}(k_{ph})]) \\ & \times\delta(\nu_{ex}(k'_{ex}) - [\nu_d + \nu_{vib}(k_{vib})])\delta(k_{ex} + k_{ph})\delta(k'_{ex} - k_{vib}) \end{aligned} \tag{19}$$

where the δ functions ensure energy and momentum conservation. The spectra shown in figure 7(b) correspond to an integration of m_0 with respect to $\boldsymbol{k}_{ph}$ and $\boldsymbol{k}_{vib}$ over the whole Brillouin zone for a fixed excitation energy ν_i. This is depicted in figure 8. Part (a) of the figure shows the excitation process. Distinct $\boldsymbol{k}$ states of the exciton bands will be populated owing to the overlap of several phonon branches. This is taken into account by

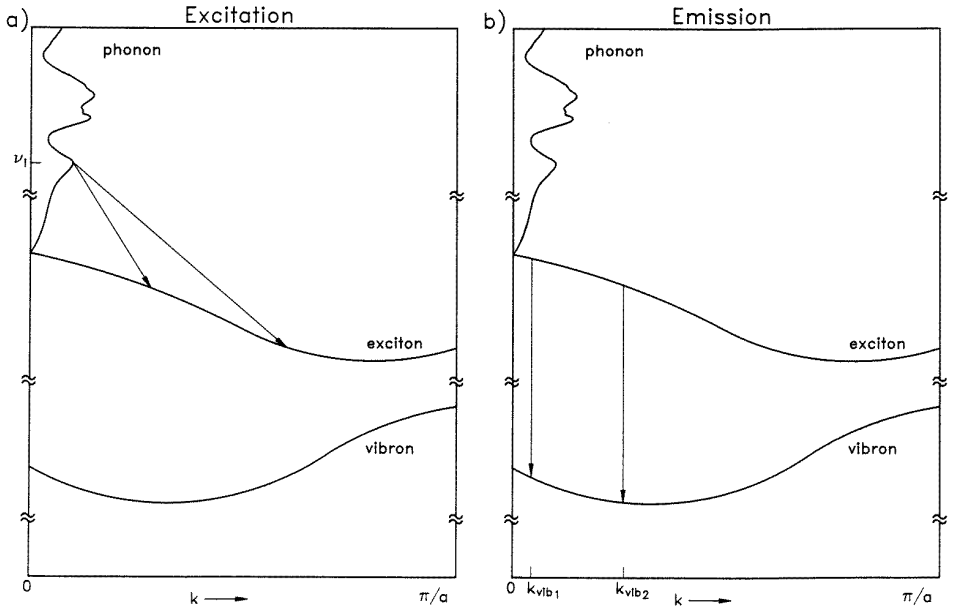

Figure 8. Excitation (a) and emission (b) processes schematically. The exciton and the vibron bandstructure in the first Brillouin zone are shown. Above the exciton resonance energy, ν_{00}, the phonon density of states is sketched (not to scale). The excitation with a photon of energy ν_i may result in the population of two (or more) distinct $\boldsymbol{k}$ states in the exciton band due to the overlap of different phonon branches at the respective excitation energy (a). Emission from different $\boldsymbol{k}$ states $\boldsymbol{k}_{vib1}$ and $\boldsymbol{k}_{vib2}$ may result in the same detection energy ν_d (b). A fluorescence spectrum as function of ν_d corresponds to an integration with respect to $\boldsymbol{k}_{vib}$ over the entire Brillouin zone.

the integration with respect to $\boldsymbol{k}_{ph}$. The detection is shown in part (b) of the figure. The detected energy corresponds to the difference in energy of the two bandstructures involved. Recording a spectrum as function of ν_d therefore means integrating with respect to $\boldsymbol{k}_{vib}$. As indicated, it can happen that for two different $\boldsymbol{k}$ states $\boldsymbol{k}_{vib1}$ and $\boldsymbol{k}_{vib2}$ the detected energies are identical. The experimental signal shown in figure 7(b) therefore corresponds to

$$\begin{aligned} M(\nu_d, \nu_i = \text{constant}) \sim \int_0^{\frac{\pi}{a}} \mathrm{d}k_{ph} \int_0^{\frac{\pi}{a}} \mathrm{d}k_{vib}\, g_{ph}(k_{ph}) g_{ex}(k_{ex}) S(k_{ex'} k'_{ex}) g_{vib}(k_{vib}) g_{ex}(k'_{ex}) \\ \times \delta(\nu_i - [\nu_{ex}(k_{ex}) + \nu_{ph}(k_{ph})]) \delta(\nu_{ex}(k'_{ex}) - [\nu_d + \nu_{vib}(k_{vib})]) \\ \times \delta(k_{ex} + k_{ph}) \delta(k'_{ex} - k_{vib}). \end{aligned} \tag{20}$$

The δ functions $\delta(\boldsymbol{k}_{ex} + \boldsymbol{k}_{ph})$ and $\delta(\boldsymbol{k}'_{ex} - \boldsymbol{k}_{vib})$ ensure that only states which fulfil $\boldsymbol{k}'_{ex} = \boldsymbol{k}_{vib}$ and $\boldsymbol{k}_{ex} = -\boldsymbol{k}_{ph}$ contribute to the signal. Therefore (20) can be written as

$$\begin{aligned} M(\nu_d, \nu_i = \text{constant}) \sim \int_0^{\frac{\pi}{a}} \mathrm{d}k_{vib} \int_0^{\frac{\pi}{a}} \mathrm{d}k_{ph} g_{ph}(k_{ph}) g_{ex}(-k_{ph}) S(-k_{ph'} k_{vib}) g_{ex}(k_{vib}) g_{vib}(k_{vib}) \\ \times \delta(\nu_i - [\nu_{ex}(-k_{ph}) + \nu_{ph}(k_{ph})]) \delta(\nu_{ex}(k_{vib}) - [\nu_d + \nu_{vib}(k_{vib})]) \end{aligned} \tag{21}$$

without changing the result. To interpret the spectra presented in figure 7(b) it was assumed that at low temperatures an exciton which is created in a particular $\boldsymbol{k}$ state will not change its quasimomentum during the entire lifetime [69]. Assuming $S(\boldsymbol{k}_{ex}, \boldsymbol{k}'_{ex}) \sim \delta(\boldsymbol{k}_{ex} - \boldsymbol{k}'_{ex})$

and substituting $\boldsymbol{k}_{ex} = -\boldsymbol{k}_{ph}$ and $\boldsymbol{k}'_{ex} = \boldsymbol{k}_{vib}$ leads to $S(\boldsymbol{k}_{ex}, \boldsymbol{k}'_{ex}) \sim \delta(-\boldsymbol{k}_{ph} - \boldsymbol{k}_{vib})$, which gives a contribution to $M(\nu_d, \nu_i = \text{constant})$ only if $-\boldsymbol{k}_{ph} = \boldsymbol{k}_{vib} = \boldsymbol{k}$. Rewriting (21) yields

$$M(\nu_d, \nu_i = \text{constant}) \sim \int_0^{\frac{\pi}{a}} \mathrm{d}k \int_0^{\frac{\pi}{a}} (-\mathrm{d}k) g_{ph}(k) g_{ex}(k) g_{ex}(k) g_{vib}(k) \times \delta(\nu_i - [\nu_{ex}(k) + \nu_{ph}(k)]) \delta(\nu_{ex}(k) - [\nu_d + \nu_{vib}(k)]). \tag{22}$$

By choosing a specific excitation energy ν_i the energy $(\nu_{ex}(\boldsymbol{k}) + \nu_{ph}(\boldsymbol{k}))$ is determined by the first δ function and therefore a finite number of exciton energies $\nu_{ex}(\boldsymbol{k})$ are selected. These select in the second δ function the energies ν_d. This means that a finite number of detection energies are determined, depending on the initial choice of ν_i, by the laser frequency. As observed the spectra depend strongly on the excitation energy.

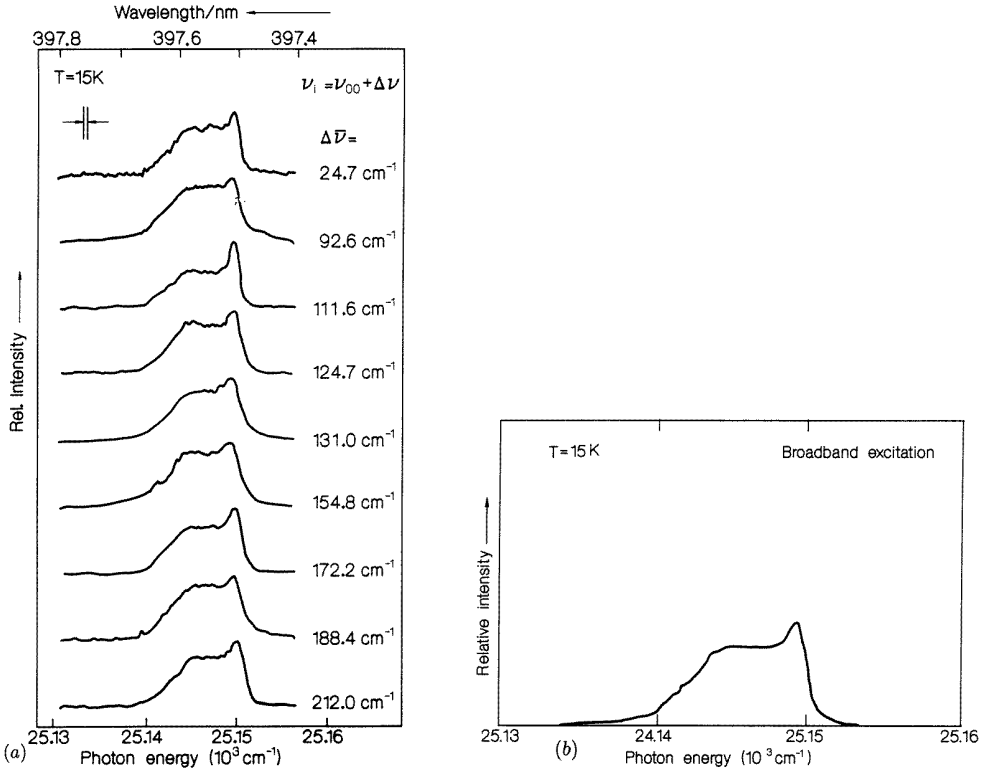

Figure 9. (*a*) The lineshape of the (0–1ν_2) fluorescence transition at 15 K for different excitation energies which correspond to those of figure 7. (*b*) For comparison, the lineshape of the (0–1ν_2) fluorescence transition at 15 K excited with a broad-band mercury arc light source [68].

In figure 9(*a*) a sequence of lineshapes of the (0–1ν_2) transition is shown, which was recorded for a crystal temperature of 15 K. The excitation energies correspond to those of figure 7(*b*). At this crystal temperature the observed lineshapes became independent of the excitation energy. Moreover the lineshape resembles that observed for broad-band excitation conditions (see figure 9(*b*)). This similarity suggests that at this temperature the whole exciton band is populated and contributes to the fluorescence transition. It was concluded that in this temperature regime an increased exciton–phonon scattering rate leads

to a redistribution of the exciton states within the manifold of $\boldsymbol{k}$ states. This corresponds to a situation where the population of states $\boldsymbol{k}'_{ex}$ becomes independent of the initial population of states $\boldsymbol{k}_{ex}$. For convenience $S(\boldsymbol{k}_{ex}\boldsymbol{k}'_{ex})$ will be approximated as a constant function $S(\boldsymbol{k}_{ex}\boldsymbol{k}'_{ex}) \sim C$. Then the $\boldsymbol{k}$ selection rules give $\boldsymbol{k}_{ex} = -\boldsymbol{k}_{ph}$ and $\boldsymbol{k}'_{ex} = \boldsymbol{k}_{vib}$, which yields for the signal

$$M(\nu_d, \nu_i = \text{constant}) \sim \int_0^{\frac{\pi}{a}} \mathrm{d}k_{vib} \int_0^{\frac{\pi}{a}} \mathrm{d}k_{ph} g_{ph}(k_{ph}) g_{ex}(-k_{ph}) C g_{vib}(k_{vib}) g_{ex}(k_{vib}) \times \delta(\nu_i - [\nu_{ex}(-k_{ph}) + \nu_{ph}(k_{ph})]) \delta(\nu_{ex}(k_{vib}) - [\nu_d + \nu_{vib}(k_{vib})]). \tag{23}$$

The two integrations are independent of each other and can be written as

$$M(\nu_d, \nu_i = \text{constant}) \sim C \left(\int_0^{\frac{\pi}{a}} \mathrm{d}k_{ph} g_{ph}(k_{ph}) g_{ex}(-k_{ph}) \delta(\nu_i - [\nu_{ex}(-k_{ph}) + \nu_{ph}(k_{ph})]) \right) \times \left(\int_0^{\frac{\pi}{a}} \mathrm{d}k_{vib} g_{vib}(k_{vib}) g_{ex}(k_{vib}) \delta(\nu_{ex}(k_{vib}) - [\nu_d - \nu_{vib}(k_{vib})]) \right). \tag{24}$$

For a fixed ν_i the first integral gives a certain value which scales the signal without any influence on the spectral dependence on ν_d. The shape of the spectra is determined (in the second integral) by the product of the density of states of the exciton and the vibron, while the δ function ensures energy conservation during the emission process. This is similar to the case of the broad-band excitation, which is exactly what has been observed.

An equivalent experimental approach is to interchange the role of ν_d and ν_i. If the detection energy is fixed and the laser energy is varied a fluorescence excitation spectrum is recorded. The result obtained for low temperatures is shown in figure 10(b). The respective detection energies, ν_d, are indicated in figure 10(a). They were chosen within the spectral regime of the fluorescence line obtained for broad-band excitation. The shape of the spectra depends strongly on the choice of the detection energy. For temperatures of 15 K and above the excitation spectra became independent of the detection energy again [70, 73]. The interpretation of the excitation spectra follows the arguments given above just by interchanging ν_i and ν_d. Although the two experiments are equivalent and based on the same underlying effect the excitation spectroscopy offered the comparison with a further independent piece of information—the excitation spectra of isotopically substituted molecules. To describe the spatially localized excited states of the isotopically substituted molecules by using Bloch states $|\boldsymbol{k}\rangle$ as basis set, one has to build wave-packets involving $\boldsymbol{k}$ states of the entire first Brillouin zone. This means that these states can be populated via the phonons independent of the phonon $\boldsymbol{k}$ vector. The excitation spectra of these molecules can be visualized as spectra of NO_2^- ions for which the $\boldsymbol{k}$ selection rule is ineffective. In other words these excitation spectra indicate the efficiency of populating these states via the phonons. This is analogous to the excitation spectra of the exciton in the rapid-thermalization regime. As shown in figure 11(a) the excitation spectrum of the isotopically substituted molecule (^{15}N natural abundance) indeed resembles in shape that of the exciton for higher temperatures (figure 11(b)). Both spectra represent an excited state which is constituted by a superposition of $|\boldsymbol{k}\rangle$ states of the whole first Brillouin zone. In the exciton case all $\boldsymbol{k}$ states are sampled because of the scattering process while the localized $\boldsymbol{k}$ states are sampled by the uncertainty relation $\Delta k \Delta x \geq 2\pi$ which yields $\Delta k \geq 2\pi/a$, for Δx of the order of the lattice constant a. A similar excitation spectrum was observed for ^{18}O substituted molecules [73].

From these experiments it can be concluded that at low temperatures the singlet excitons in $NaNO_2$ conserve their initial $\boldsymbol{k}$ vector and a wavelike description of the excitons (coherent limit) is adequate [70, 73].

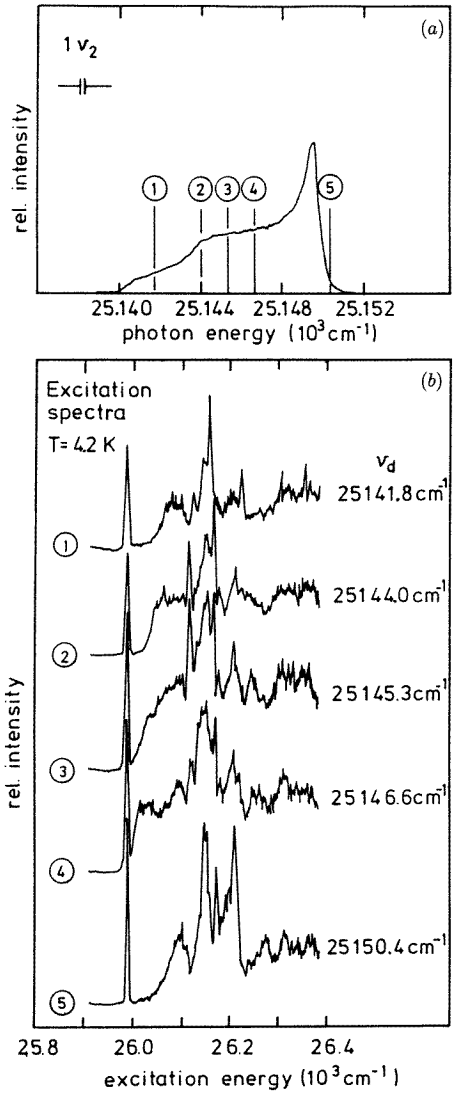

Figure 10. The fluorescence excitation spectrum (*b*) of the (0–1ν_2) transition at 4.2 K. For comparison the detection energies, ν_d, are labelled 1–5 within the lineshape of the fluorescence transition (*a*) which is obtained if the sample is excited with a broad-band light source.

5.2.2. Time resolved experiments. In the previous subsection the fluorescence lineshapes were discussed for the two limiting cases $S \sim \delta(\boldsymbol{k} - \boldsymbol{k}')$ and $S \sim C$. This section is concerned with intermediate temperatures and the temporal evolution of the function S on a nanosecond timescale which reflects the redistribution of the excitons within the Brillouin zone [70]. The sample was excited with a laser flash of 3 ns duration (FWHM) and an excess energy of 18 cm^{-1} above the exciton resonance. The excitons created have $\boldsymbol{k}$ vectors close to $\boldsymbol{k} = \boldsymbol{0}$. The fluorescence was detected during a well defined time interval, called a 'gate' in the following. The gate width was chosen to be 5 ns and could be delayed with respect to the laser flash giving insights into the dynamics of the exciton population. The

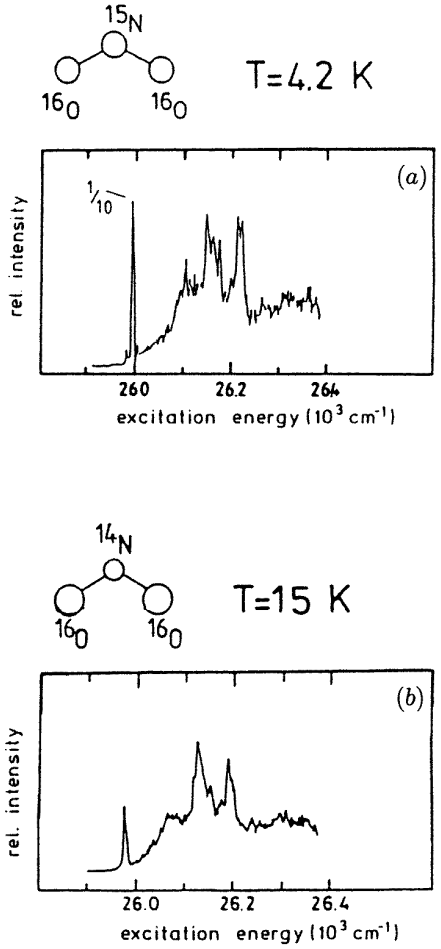

Figure 11. Fluorescence excitation spectra of the (0–1ν_2) transition for (*a*) ^{15}N substituted molecules (natural abundance) at 4.2 K and (*b*) the singlet exciton at 15 K.

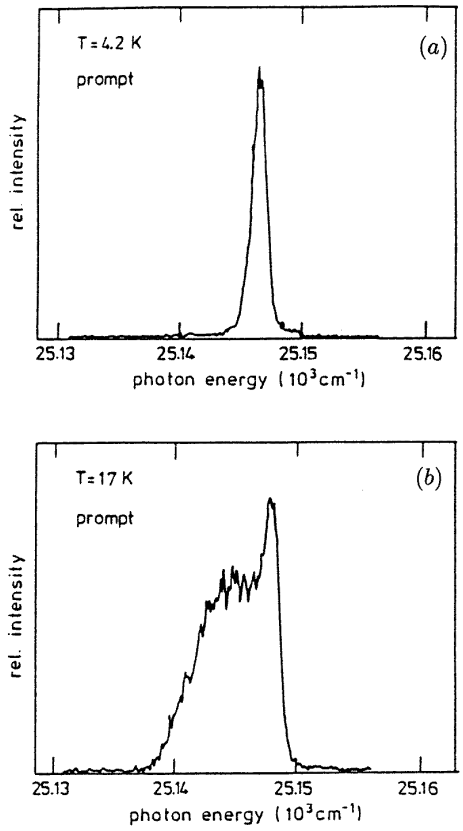

Figure 12. The lineshape of the (0–1ν_2) fluorescence transition at 4.2 K (*a*) and 17 K (*b*). The excitation energy corresponded to an excess energy of $\Delta\nu$ = 18 cm^{-1}. The fluorescence was detected only during the first 5 ns after the laser flash [70].

signal recorded for a delay $\Delta t = 0$ will be called 'prompt'. To monitor the fluorescence the (0–1ν_2) transition was chosen. In figure 12 the prompt signals for the two limiting temperature regimes are compared. For low temperature (figure 12(*a*)), a symmetric line at a position of $\nu = (25\,146.3 \pm 0.5)$ cm^{-1} and a width of 1.3 cm^{-1} (FWHM) was observed. At higher temperatures (figure 12(*b*)), the lineshape of the prompt signal already resembles that obtained under broad-band excitation conditions at the same temperature. In figure 13 the transition between the two limiting cases is shown. In the left-hand part of the figure a sequence of spectra recorded at 11.5 K is shown. The delay Δt increases stepwise from the bottom to the top. The prompt signal still shows a significant deviation from the 'broad-band lineshape' which is shown for comparison in the inset of figure 13 for the same temperature. However, for a delay of 35 ns the lineshape obtained at 11.5 K is similar to the 'broad-band lineshape'. Increasing the temperature, as illustrated in the right-hand part of figure 13,

results in a shorter delay necessary to obtain the thermalized lineshape. These experiments confirmed that at low temperatures the thermalization of the exciton band lasts a long time with respect to the exciton decay time of 8 ns.

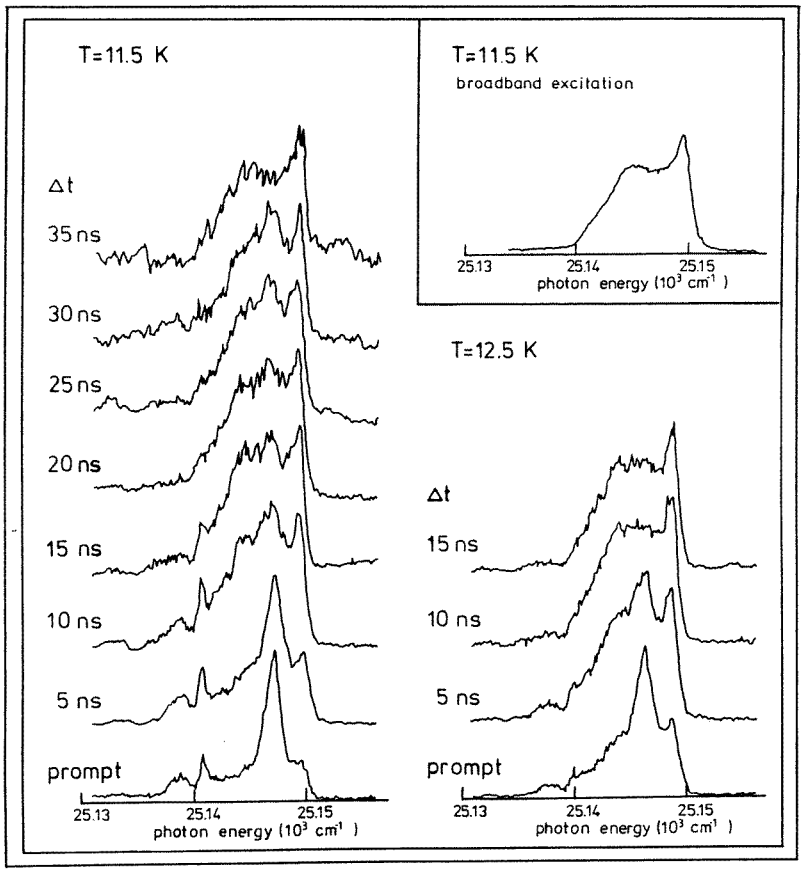

Figure 13. The dependence of the lineshape of the $(0–1\nu_2)$ fluorescence transition on the delay, Δt, between the exciting laser flash and the detection gate. The sequences displayed were recorded at 11.5 K (left) and 12.5 K (right). For comparison the corresponding lineshape for broad-band excitation conditions is shown in the inset [70].

5.3. The thermalization process

The time resolved experiments allowed a crude determination of the time necessary for the excitons to thermalize. The thermalization time was estimated by the shortest delay Δt that was necessary to obtain the 'broad-band lineshape' [70]. It was concluded that at 4.2 K the thermalization time is much longer than 35 ns because no change of the lineshape was observed within the accessible delay. In figure 14 the estimates for the inverse of the thermalization time as obtained from the delays for various temperatures are shown. By taking advantage of well known properties of $NaNO_2$ such as the phonon dispersion relations [31, 32], the temperature dependence of the specific heat [33] and the elastic constants [85], it was concluded that the exciton thermalization is determined by Raman-like two-phonon

scattering events [70]. This means scattering events in which one phonon is annihilated and another one is emitted. For acoustic phonon scattering a T^7 temperature dependence of the thermalization rate is expected [86] while for optical phonons an exponential temperature dependence should be observed [87]. Following a pragmatic approach as suggested in [88] the curve shown in figure 14 is based on a function of the form

$$\tau^{-1} = \tau_0^{-1} + a(T/\theta_D)^7 + b\exp(-E_{phonon}/kT) \tag{25}$$

using the values of 120 cm^{-1} for E_{phonon}, which is the energy of the lowest optical mode in $NaNO_2$, and 345 K for the Debye temperature, θ_D. The parameters a and b were adjusted to fit the observed data points. For a better comparison the broken curve in figure 14 gives the T^7 term only. The result of this approach is that a reasonable agreement with the experiment can be achieved only by allowing optical and acoustic phonon scattering to be relevant [70].

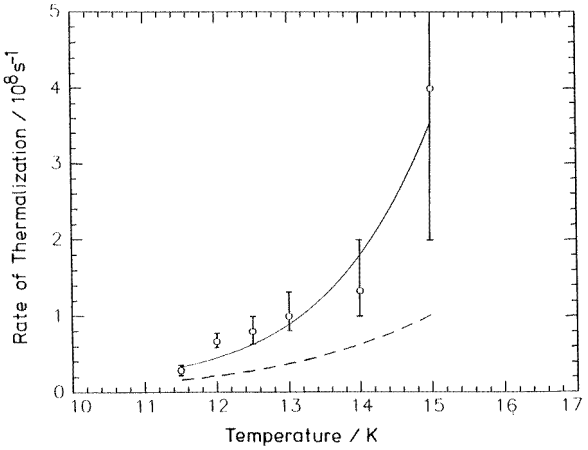

Figure 14. The rate of thermalization as obtained from the lineshape studies. The full line corresponds to a calculation according to equation (25) using $\tau_0^{-1} = 10^7\ s^{-1}$, $a = 3.5\times10^{17}\ s^{-1}$, $b = 2.5\times10^{13}\ s^{-1}$, $\theta_D = 345$ K and $E_{phonon} = 120\ cm^{-1}$. The broken curve represents the part $\tau^{-1} \sim a(T/\theta_D)^7$ only [70].

Ashida and Kato [89] studied the energy transfer from resonantly excited isotopically substituted molecules to the exciton band. They observed an increase in the exciton fluorescence intensity with raising temperature. In contrast to the exciton thermalization this could be explained with a two-phonon Raman-like process of acoustic phonons only. Due to the localized character of the excited states of the isotopically substituted molecules the $\boldsymbol{k}$ conservation is lifted and only energy conservation has to be taken into account. Therefore the result of this study cannot be adapted directly for the exciton thermalization. Nevertheless it shows that even for this less restrictive case concerning the conservation rules the contribution of one-phonon scattering to the thermalization is negligible.

5.4. Exciton coherence

A realistic description of the intermediate case between purely coherent wavelike excitons and a 'hopping' quasiparticle can be attempted by representing the excitation as a wave-packet. The lifetime of any particular $\boldsymbol{k}$ state contributing to this packet is limited because of the finite lifetime of the excited state and because the exciton can be scattered into another

$\boldsymbol{k}$ state. As was pointed out the excitons conserve their $\boldsymbol{k}$ vector at low temperatures, which means that the constitution of the wave-packet is not changed significantly during the exciton lifetime. At 11.5 K the '$\boldsymbol{k}$ state memory time' can be estimated as [90]

$$[\tau(k)]^{-1} = (1/8\ \text{ns} + 1/35\ \text{ns}) = 1/6.5\ \text{ns}. \tag{26}$$

This time can be regarded as a characteristic time for changes of the constitution of the wave-packet. It should be compared with the intermolecular transfer time F^{-1} which is the time it takes for the wave-packet as a whole to move for one lattice site. The value obtained for F^{-1} was about 6.5 ps [52]. This means that the wave-packet visits about 1000 lattice sites before it changes its constitution significantly. From these arguments it was concluded that the exciton motion in $NaNO_2$ is wavelike to a high degree of coherence, at least below 11.5 K.

6. Quasibound vibrational states

So far a consistent model has been proposed to explain the lineshapes observed in fluorescence. In phosphorescence studies, on the other hand, the transitions of the triplet exciton to the vibrationally excited states of the electronic ground state yielded lineshapes depending on the number of vibrational quanta involved. This has been observed already by Lisse *et al* [51] and it was studied in detail for the first members of the progression by Kato *et al* [91] (see figure 15). As expected from the previous sections the (0–0) line is symmetric and has a Lorentzian profile, the linewidth of which is 0.5 cm^{-1}. Due to the $\boldsymbol{k}$ conservation rule this transition is possible only for excitons with $\boldsymbol{k} = \boldsymbol{0}$ since no vibron is created in the ground state. For the (0–1ν_2) transition an asymmetric lineshape is observed, which served to estimate the vibron bandwidth. The shape of this line is in agreement with the density of states calculated for the ν_2 vibron band. Obviously the higher members of the progression show deviations from this lineshape. A relatively narrow peak (0.6 cm^{-1}) with weak sidebands on the lower-energy side is observed for the (0–2ν_2) triplet transition. Because the influence of the exciton bandstructure on the lineshape can be neglected for the triplet transitions the features observed have to be attributed to the vibrons.

If the vibrations in the crystal were purely harmonic, the excitation energy of a doubly excited vibrational state would be exactly the same as twice the energy of the fundamental state. For vibrons this means that there is no difference in energy of two fundamental vibrons travelling independently through the crystal (a two-vibron state) and a vibron in which each molecule is doubly excited (an overtone state). If the molecular vibration is anharmonic the ratio of these energies determines what is going to happen. If the anharmonicity is large a so-called bivibron state is formed, which has small coupling to the states in the two-vibron band. An overtone vibration travels through the crystal. If the anharmonicity is small compared to the bandwidth there is a strong coupling between the overtone and the two-vibron states. The energy of the bivibron lies in the two-vibron band. The theory of multivibron bound states has been studied intensively in recent years [92–99]. To obtain the anharmonicity for the ν_2 vibron of $NaNO_2$ accurate values for the peak positions of the luminescence lines have been determined. From these figures the anharmonicity constant $A = (E_0 - \frac{1}{2}E_2)$ of the ν_2 vibration has been obtained [91], where E_0 is the energy of the fundamental mode and E_2 is the energy of the first overtone. The value obtained for A is (0.8 ± 0.5) cm^{-1}. The accuracy of A is rather poor because it is the difference of two large numbers. The full bandwidth of the ν_2 vibron band has been estimated to be about 3 cm^{-1} [68], a value consistent with that given in [91] of (1.7 ± 0.5) cm^{-1}. The anharmonicity and the bandwidth are of the same order of magnitude and it cannot be expected that a bivibron

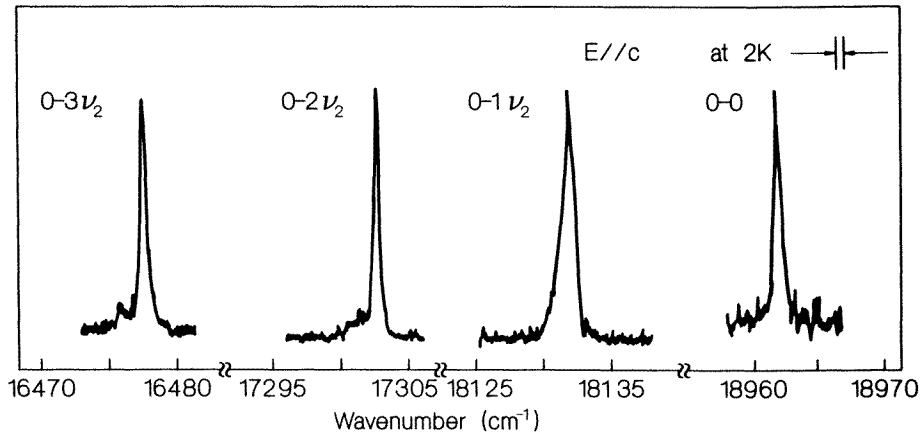

Figure 15. The lineshapes of the first members of the ν_2 progression in the phosphorescence spectrum [91].

state is formed with energies distinct from that of the two-vibron states. Following the model calculation of Belousov [96] for this case a two-vibron quasibound state instead of a bivibron can be formed, located at the bottom of the two-vibron band. Therefore the narrow peak of the (0–2ν_2) triplet luminescence lines is ascribed to the quasibound state while the low-energy sideband corresponds to the two-vibron dissociated state. That the quasibound state which is located at the bottom of the two-vibron band appears on the high-energy side of the spectra is due to the fact that in the luminescence spectra the energy difference between the initial and the final state is measured. Therefore the energy difference is largest for states near the bottom of the band of final states. Using the same model potential as for the bandstructure calculations Janssen and van der Avoird [100] computed the bivibron and quasibound vibron states. The lineshape calculated depends strongly on the value used for the anharmonicity constant A. For $A = 0.3$ cm^{-1} the overtone state is strongly coupled to the two-vibron band and not visible in the spectrum. For $A = 0.8$ cm^{-1} in the calculations of Janssen and van der Avoird a quasibound state began to show up, whereas for $A = 1.3$ cm^{-1} a well pronounced quasibound state was predicted in the spectrum together with a weak shoulder. The calculated lineshape obtained for $A = 1.3$ cm^{-1} is compared in figure 16 with the lineshapes of the (0–2ν_2) transition.

In the fluorescence spectra the influence of the coupled state on the lineshape was completely masked by the contribution of the singlet exciton dispersion to the lineshape. However there are two possibilities of 'switching off' the singlet exciton bandstructure. Recording (resonant) Raman scattered light involves only states at $\boldsymbol{k} = \mathbf{0}$; the final state of this process can be the quasibound state. Another possibility is to take advantage from the slow redistribution of $\boldsymbol{k}$ states in the exciton band at low temperatures. Exciting the crystal with a narrow-band laser close to $\boldsymbol{k} = \mathbf{0}$ offers the possibility of studying the quasibound states. In figure 17 the fluorescence lineshape of the (0–2ν_2) transition for near-resonant excitation is compared with the calculated lineshape. The Raman scattering experiment yields a similar result and is not shown here. The experimental line shows a narrow peak of about 1.4 cm^{-1} width (the respective spectral width of the laser was 1.2 cm^{-1}) and a shoulder on the lower-energy side. This experiment demonstrates that the quasibound states are also observable in fluorescence. In conclusion it can be stated that the observed features

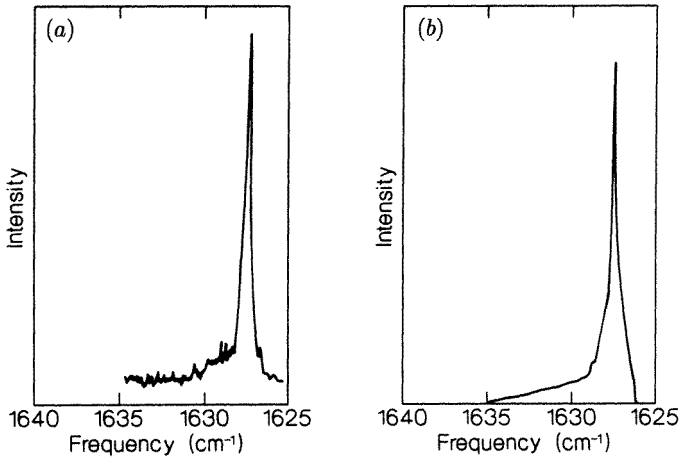

Figure 16. Experimental (*a*) and calculated (*b*) lineshapes of the (0–$2\nu_2$) phosphorescence transition. For the calculation $A = 1.3\ \mathrm{cm}^{-1}$ was used [91, 100].

are very well compatible with the interpretation of quasibound vibron states. The value used for A in the calculations is slightly larger than the experimental value but still consistent within the experimental error.

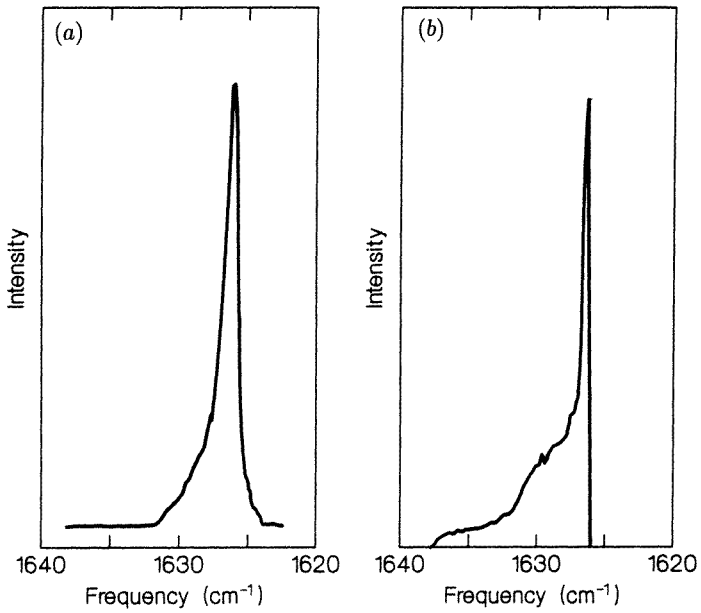

Figure 17. A comparison of experimentally (*a*) and theoretically (*b*) obtained lineshapes. (*a*) The lineshape obtained for the (0–$2\nu_2$) fluorescence transition for narrow-band excitation close to ν_{00} at low temperatures [91]. (*b*) The calculated lineshape for $A = 1.3\ \mathrm{cm}^{-1}$ [100].

7. Summary

This contribution summarizes the investigation of excitation energy transfer and luminescence lineshape studies carried out on pure and potassium doped $NaNO_2$ crystals. The energy transfer in $NaNO_2$ is determined by the motion of the excitons and not by the capture process at trap states. This makes $NaNO_2$ a suitable system to study the motion of Frenkel excitons. From the analysis of the data in terms of a generalized master equation approach it is concluded that a one-dimensional exciton motion is most probable.

In agreement with these conclusions are the results from a detailed study of the luminescence lineshapes observed. The asymmetric lineshape of the fluorescence transitions is predominantly ascribed to the dispersion of the singlet exciton and that of the vibron involved in the transition. For lower temperatures this lineshape additionally depends on the excitation conditions. This is due to the slow redistribution of the exciton $\boldsymbol{k}$ states in the Brillouin zone. The thermalization of the exciton band is explained by a simple exciton–phonon scattering model. A minor influence on the lineshape is given by the formation of quasibound states in the overtone bands of the vibron bandstructures. This effect can be studied most easily for the triplet transitions (phosphorescence) where the influence of the triplet exciton dispersion is negligible, but it can also be observed in the fluorescence spectra. It can be stated that the lineshape of the luminescence transitions of $NaNO_2$ is understood in a consistent way.

Acknowledgments

We would like to thank M Ashida, A van der Avoird, W B J M Janssen and R Kato for many fruitful discussions and collaborations.

References

[1] Frenkel J 1931 *Phys. Rev.* **37** 17
[2] Davydov A S 1971 *Theory of Molecular Excitons* (New York: Plenum)
[3] Wolf H C 1967 *Adv. At. Mol. Phys.* **3** 119
[4] Robinson G W 1970 *Annu. Rev. Phys. Chem.* **21** 429
[5] Powell R C and Soos Z G 1975 *J. Lumin.* **11** 1
[6] Burland D M and Zewail A H 1979 *Adv. Chem. Phys.* **40** 369
[7] Pope M and Swenberg C E 1982 *Electronic Processes in Organic Crystals* (Oxford: Oxford University Press)
[8] Fayer M D 1983 *Spectroscopy and Excitation Dynamics of Condensed Molecular Systems* ed V M Agranovich and R M Hochstrasser (Amsterdam: North-Holland) p 185
[9] Schmidt J 1989 *Relaxation Processes in Molecular Excited States* ed J Fünfschilling (Dordrecht: Kluwer) p 51
[10] Knox R S 1963 *Theory of Excitons* (New York: Academic)
[11] Ziegler G E 1931 *Phys. Rev.* **38** 1040
[12] Kay M I, Gonzalo J A and Maglic R 1975 *Ferroelectrics* **9** 179
[13] Kucharzyk D, Pietrasko A and Lukaszewiecz K 1976 *Phys. Status Solidi* a **37** 287
[14] Sack H S and Moriarty M C 1965 *Solid State Commun.* **3** 93
[15] Sidman J 1957 *J. Am. Chem. Soc.* **79** 2669
[16] Chisler E V and Shur M S 1966 *Phys. Status Solidi* **17** 163
[17] Hartwig C M, Wiener-Avnear E and Porto S P S 1981 *Phys. Rev.* B **23** 3748
[18] Tsuboi M, Terada M and Kajiura T 1969 *Bull. Chem. Soc. Japan* **42** 1871
[19] Asawa C K and Barnoski M K 1970 *Phys. Rev.* B **2** 205
[20] Castellucci E and Schettino V 1979 *Phys. Status Solidi* b **91** 641
[21] Becucci M and Castellucci E 1989 *Chem. Phys.* **135** 363
[22] Castellucci E, Firstein L and Porto S P S 1976 *Int. Conf. on Light Scattering in Solids (Campinas, 1975)* vol 3, ed M Balkanski (Paris: Flammarion) p 872

[23] Prasad-Rao A D and Porto S P S 1976 *Int. Conf. on Light Scattering in Solids (Campinas, 1975)* ed M Balkanski (Paris: Flammarion) p 87
[24] Goncharuk I N, Davydov V Yu, Ivanova E A and Chisler E V 1978 *Sov. Phys.–Solid State* **20** 1676
[25] Hollah G D 1971 *J. Phys. C: Solid State Phys.* **4** 2191
[26] Kamada M, Yoshikawa M and Kato R 1975 *J. Phys. Soc. Japan* **39** 1004
[27] Vogt H and Happ H 1966 *Phys. Status Solidi* **16** 711
[28] Axe J D 1968 *Phys. Rev.* **167** 573
[29] Barnoski M and Ballantyne J M 1968 *Phys. Rev.* **174** 946
[30] Brehat F and Wyncke B 1985 *J. Phys. C: Solid State Phys.* **18** 1705
[31] Sakurai J, Cowley R A and Dolling G 1970 *J. Phys. Soc. Japan* **28** 1426
[32] Dolling G, Sakurai J and Cowley R A 1970 *J. Phys. Soc. Japan* Suppl. **28** 258
[33] Villar R, Gmelin E and Grimm H 1986 *Ferroelectrics* **69** 165
[34] Carsey T P and McGlyn S P 1979 *J. Am. Chem. Soc.* **101** 1728
[35] Aavikso Ya Yu, Aniyalg A O, Saari P M and Soovik T A 1977 *Sov. Phys.–Solid State* **19** 477
[36] Hangyo M, Yamanaka H and Kato R 1980 *J. Phys. Soc. Japan* **50** 895
[37] Clark S E and Tinti D S 1979 *Chem. Phys. Lett.* **60** 292
[38] Clark S E and Tinti D S 1980 *Chem. Phys.* **51** 17
[39] Kokai F and Azumi T 1982 *J. Phys. Chem.* **86** 177
[40] Maria H J, Armstrong A T and McGlyn S P 1968 *J. Chem. Phys.* **48** 4694
[41] Hochstrasser R M and Marchetti A P 1969 *J. Chem. Phys.* **50** 1727
[42] Dietrich W, Drissler F, Schmid D and Wolf H C 1973 *Z. Naturf.* a **28** 284
[43] Kamada M and Kato R 1978 *J. Phys. Soc. Japan* **45** 169
[44] van der Waals J H and de Groot M S 1967 *The Triplet State* ed A B Zahlan (New York: Cambridge University Press) p 101
[45] Schmidt J and van der Waals J H 1979 *Time Domain Electron Spin Resonance* ed L Kevan and R N Schwartz (New York: Wiley) p 343
[46] Dietrich W 1975 *PhD Thesis* Stuttgart
Dietrich W and Schmid D 1976 *Phys. Status Solidi* b **74** 609
[47] Dietrich W, Schmidt L and Schmid D 1974 *Chem. Phys. Lett.* **28** 249
[48] von Schütz J and Dietrich W 1977 *Chem. Phys. Lett.* **51** 418
[49] Rodloff G 1934 *Z. Phys.* **91** 511
[50] Ashida M, Kawaguchi Y and Kato R 1989 *J. Phys. Soc. Japan* **58** 4620
[51] Lisse F 1985 *PhD Thesis* Düsseldorf
Lisse F, Köhler J, Pufahl H and Schmid D 1987 *Phys. Status Solidi* b **140** 605
[52] Pufahl H 1986 *PhD Thesis* Düsseldorf
Pufahl H, Köhler J, Schmidt Th, Schmid D and Kenkre V M 1987 *Phys. Status Solidi* b **141** 303
[53] Kenkre V M and Reineker P M 1982 *Exciton Dynamics in Molecular Crystals and Aggregates (Springer Tracts in Modern Physics 94)* ed G Höhler (Berlin: Springer)
[54] Kenkre V M, Parris P E and Schmid D 1985 *Phys. Rev.* B **32** 4946
[55] Kenkre V M and Schmid D 1983 *Chem. Phys. Lett.* **94** 603
[56] Kenkre V M and Knox R S 1974 *Phys. Rev.* B **9** 5279
[57] Kenkre V M 1983 *Organic Molecular Crystals* ed P M Reineker (Berlin) p 193
[58] Kenkre V M 1981 *Z. Phys.* B **43** 221
[59] Kenkre V M 1980 *Phys. Rev.* B **22** 2089
[60] Kenkre V M and Parris P E 1983 *Phys. Rev.* B **27** 3221
[61] Kenkre V M 1984 *Energy Transfer Processes in Condensed Matter* ed B di Bartolo (New York) p 205
[62] Pröpstl A and Wolf H C 1963 *Z. Naturf.* a **18** 724
[63] Port H and Wolf H C 1968 *Z. Naturf.* a **23** 315
[64] Schmidt L 1978 *PhD Thesis* Stuttgart
[65] Schmidt L, Port H and Schmid D 1977 *Chem. Phys. Lett.* **51** 413
[66] Ohta O and Kato R 1993 *Proc. XII Int. Conf. on Defects in Insulating Materials (Schloß Nordkirchen, 1992)* vol I, ed O Kanert and J-M Spaeth (Singapore: World Scientific) p 1072
[67] Schmidt Th 1987 *PhD Thesis* Düsseldorf
Schmidt Th, Köhler J, Kryschi C and Schmid D 1988 *Phys. Status Solidi* b **147** 797
[68] Köhler J, Ashida M, Kato R, Schmidt Th and Schmid D 1991 *J. Lumin.* **47** 239
[69] Köhler J, Hucke M, Schmid D, Ashida M and Kato R 1992 *J. Lumin.* **53** 76
[70] Köhler J, Hucke M and Schmid D 1992 *J. Lumin.* **52** 293
[71] Kawaura H, Kawaguchi Y and Kato R 1988 *J. Phys. Soc. Japan* **57** 3613

[72] Kato H, Yonezawa T, Morukuma K and Fukui K 1964 *Bull. Chem. Soc. Japan* **37** 1710
[73] Köhler J, Schmidt Th and Schmid D 1990 *J. Mol. Struct.* **219** 37
[74] Köhler J 1986 *Diplomarbeit* Düsseldorf
[75] Yamanaka Y, Hangyo M and Kato R 1981 *J. Phys. Soc. Japan* **50** 2689
[76] Kobayashi T and Kato R 1984 *J. Phys. Soc. Japan* **53** 2157
[77] Janssen W B J M, van der Avoird A, Köhler J and Schmid D 1992 *Phys. Status Solidi* b **173** 587
[78] Dolling G 1969 *Molecular Dynamics and Structure of Solids (National Bureau of Standards Special Publication 301)* ed R S Carter and J J Rush (Gaithersburg, MD: National Bureau of Standards)
[79] Castellucci E and Schettino V 1980 *J. Mol. Struct.* **61** 191
[80] Lynden-Bell R M, Impey R W and Klein M L 1986 *Chem. Phys.* **109** 25
[81] Hirutsu S, Yanagi T and Sawada S 1968 *J. Phys. Soc. Japan* **25** 799
[82] Köhler J, Schmid D, Ashida M, Kato R, Jannsen W B J M and van der Avoird A 1992 *World Scientific: Special Issue ICDIM '92* vol II, ed O Kanert and J-M Spaeth (Singapore: World Scientific) p 1069
[83] Sakai T, Kawaura H and Kato R 1987 *J. Phys. Soc. Japan* **56** 1943
[84] Kamada M, Yoshimura T and Kato R 1977 *J. Phys. Soc. Japan* **42** 1660
[85] Ota K and Ishibashi Y 1970 *J. Phys. Soc. Japan* **29** 1545
[86] McCumber D E and Sturge M D 1963 *J. Appl. Phys.* **34** 1682
[87] Munn R W and Silbey R 1980 *Mol. Cryst. Liq. Cryst.* **57** 131
[88] Port H, Nissler H and Silbey R 1987 *J. Chem. Phys.* **87** 1994
[89] Ashida M and Kato R 1992 *World Scientific: Special Issue ICDIM '92* vol II, ed O Kanert and J-M Spaeth (Singapore: World Scientific) p 1072
[90] Harris C B and Zweemer D A 1978 *Annu. Rev. Phys. Chem.* **29** 473
[91] Kato R, Ashida M, Köhler J and Schmid D 1991 *Phys. Lett.* **157A** 435
[92] Agranovich V M and Lalov I I 1985 *Sov. Phys.–Usp.* **28** 484
[93] Agranovich V M, Dubowski O A and Orlov A V 1986 *Phys. Lett.* **119A** 83
[94] Agranovich V M, Dubowski O A and Orlov A V 1989 *Solid State Commun.* **70** 675
[95] Agranovich V M, Dubowski O A and Orlov A V 1989 *Solid State Commun.* **72** 491
[96] Belousov M V 1986 *Excitons* (selected papers) ed E I Rashba and M D Sturge (Amsterdam: North-Holland) ch 9, p 395
[97] Kimball J C, Fong C Y and Shen Y R 1981 *Phys. Rev.* B **23** 4946
[98] Bogani F 1987 *J. Phys. C: Solid State Phys.* **11** 1283
[99] Bogani F 1987 *J. Phys. C: Solid State Phys.* **11** 1297
[100] Janssen W B J M and van der Avoird A 1992 *Phys. Rev.* B **46** 831